SIAM J. SCI. COMPUT.
Vol. 21, No. 5, pp. 1706–1727
© 2000 Society for Industrial and Applied Mathematics

FIRST-ORDER SYSTEM LEAST SQUARES FOR LINEAR ELASTICITY: NUMERICAL RESULTS*

Z. CAI†, C.-O. LEE‡, T. A. MANTEUFFEL§, AND S. F. MCCORMICK§

Abstract. Two first-order system least squares (FOSLS) methods based on L^2 norms are applied to various boundary value problems of planar linear elasticity. Both use finite element discretization and multigrid solution methods. They are *two-stage* algorithms that solve first for the displacement flux variable (the gradient of displacement, which easily yields the deformation and stress variables), then for the displacement variable itself. As a complement to a companion theoretical paper, this paper focuses on numerical results, including finite element accuracy and multigrid convergence estimates that confirm uniform optimal performance—even as the material tends to the incompressible limit.

Key words. elasticity equations, first-order system least squares, Lamé constants, multigrid

AMS subject classifications. 65F10, 65N55, 73V05

PII. S1064827598338640

1. Introduction.

We apply first-order system least squares (FOSLS) based on L^2 norms to planar linear elasticity problems with displacements in $H^{2+\alpha}$ for some $\alpha > 0$. (Less regular problems can be treated by FOSLS based on H^{-1} norms, but we leave this to future study.) Accordingly, let Ω be a convex polygon or a $C^{1,1}$ domain in $\mathbb{R}^2$ with boundary Γ. Denote the Lamé constants by μ and λ, where $(\mu, \lambda) \in [\mu_1, \mu_2] \times (0, \infty)$ for fixed positive constants μ_1 and μ_2. The planar linear elasticity equations with mixed boundary conditions can be written as

$$
\begin{aligned}
-\mu\Delta\mathbf{u} - (\lambda+\mu)\nabla\nabla\cdot\mathbf{u} &= \mathbf{f} \quad \text{in} \quad \Omega\,, \\
\sum_{j=1}^{2} \sigma_{ij}(\mathbf{u}) n_j &= 0 \quad \text{on} \quad \Gamma_T, \quad 1 \le i \le 2\,, \\
\mathbf{u} &= \mathbf{0} \quad \text{on} \quad \Gamma_D\,.
\end{aligned} \tag{1}
$$

Here we use the following notation: the symbols Δ, ∇, and $\nabla\cdot$ stand for the Laplacian, gradient, and divergence operators, respectively ($\Delta\mathbf{u}$ is the vector of components Δu_i); $\mathbf{u} = (u_1, u_2)^t$ denotes the displacement, $\mathbf{f} = (f_1, f_2)^t$ is a given body force, and $\mathbf{n} = (n_1, n_2)^t$ is the outward unit normal on the boundary; $\sigma_{ij}(\mathbf{u}) = \lambda(\nabla\cdot\mathbf{u})\delta_{ij} + 2\mu\epsilon_{ij}(\mathbf{u})$ is the *stress tensor*, $\epsilon_{ij}(\mathbf{u}) = \frac{1}{2}(\partial_j u_i + \partial_i u_j)$ is the *strain tensor*, and δ_{ij} is the Kronecker delta symbol; and the boundary $\Gamma = \Gamma_T \cup \Gamma_D$, where $\Gamma_T \cap \Gamma_D = \emptyset$. If $\Gamma_D = \emptyset$, then (1) is called the *pure traction problem*; if $\Gamma_T = \emptyset$, then (1) is called the *pure displacement problem*; otherwise, (1) is called the *mixed boundary value problem*.

*Received by the editors May 13, 1998; accepted for publication (in revised form) March 3, 1999; published electronically April 28, 2000.

http://www.siam.org/journals/sisc/21-5/33864.html

†Department of Mathematics, Purdue University, 1395 Mathematical Sciences Building, West Lafayette, IN 47907-1395 (zcai@math.purdue.edu). This work was sponsored by National Science Foundation grant DMS-9619792.

‡Math Department, Inha University, Inchon 402-751, Korea (colee@math.inha.ac.kr). This work was sponsored by grants BSRI-97-1436 and KOSEF 97-0701-01-01-3.

§Applied Math Department, Campus Box 526, University of Colorado at Boulder, Boulder, CO 80309-0526 (tmanteuf@boulder.colorado.edu, stevem@boulder.colorado.edu). The work of the third and fourth authors was sponsored by National Science Foundation grant DMS-9706866 and Department of Energy grant number DE-FG03-93ER25165.

It is well known that standard Galerkin finite element formulations using piecewise linear (P_1) elements are accurate for moderate values of λ, but, as $\lambda \to \infty$ (i.e., the elastic material becomes nearly incompressible), their approximation properties degrade severely [1, 15]. To overcome this so-called *locking problem*, several alternate formulations have been studied [2, 11, 12, 14], typically based on *mixed* forms of (1) that lead to discrete equations that can be difficult to solve. More recently [7], FOSLS was developed for solving the generalized Stokes equation that applies to the pure displacement problem of linear elasticity, and a direct FOSLS approach was developed in [8] for the pure traction problem. Both FOSLS formulations exhibit H^1 equivalence (continuity and coercivity) of the homogeneous part of the least-squares functional *uniformly* in λ, which guarantees optimal finite element accuracy and multigrid convergence independent of λ.

In this paper, we study the performance of multigrid methods for solving the linear systems that arise from applying standard (i.e., bilinear) finite elements to these two FOSLS formulations of various boundary value problems of planar linear elasticity. Both formulations, one based on the least-squares functional for the pure traction problem developed in [8] and the second based on the least-squares functional for the generalized Stokes equation developed in [7], are *two-stage* in that they solve first for the displacement flux, then for displacement itself. This second step is a fairly straightforward problem involving two separate Poisson-like problems, so we concentrate here on analyzing performance of the first stage.

These two-stage FOSLS approaches were first analyzed individually in [7, 8]. In a companion paper [6], we study how they relate to each other from a theoretical standpoint by establishing λ-uniform equivalence between the two algorithms for both pure traction and pure displacement boundary conditions. This has the effect of proving λ-uniform performance of standard finite element discretization and multigrid solution methods applied to *either* FOSLS approach for *either* of the pure boundary condition cases.

The present paper attempts to confirm this theory numerically. We show here, for solutions that are sufficiently smooth, that finite element approximations using bilinear elements on uniform grids converge to the exact solution with $O(h^2)$ error in the L^2 norm and $O(h^2)$ error in the functional norm. Since the functional norm is equivalent to the H^1 norm, this latter rate is faster than what is predicted by the theory in [6, 7, 8], but it is consistent with similar behavior for a least-squares formulation of the Helmholtz equations observed in [9]. For pure traction on the unit square, we show that a $\mathsf{V}(1,1)$ cycle with extra smoothing at the boundary yields asymptotic convergence factors of approximately 0.42, independent of λ and h, and that full multigrid computes a final approximation with accuracy on the order of discretization error in a total amount of work equal to about 11 relaxation sweeps on the finest grid. For pure displacement and mixed boundary conditions, we show that a $\mathsf{W}(1,0)$ cycle yields asymptotic convergence factors of approximately 0.66, independent of λ and h, and that full multigrid computes a final approximation with accuracy on the order of discretization error in a total amount of work equal to about 16 relaxation sweeps on the finest grid.

Theoretical foundation for the classical equations of linear elasticity can be found in [2, 3, 4, 13]. A description of basic multigrid algorithms and principles can be found in [5].

This paper is organized as follows. In section 2, we introduce notation and define the spaces on which we pose our formulations. Two FOSLS approaches are introduced

in section 3. In section 4, we describe the multigrid algorithm and, in section 5, we present the results of various numerical experiments. The last section is devoted to some conclusions and final remarks.

2. Preliminaries. We use standard notation and definitions for the Sobolev spaces $[H^k(\Omega)]^2$, associated inner products $(\cdot,\cdot)_k$, and respective norms $\|\cdot\|_k$, $k>0$. The space $[L^2(\Omega)]^2$ is interpreted as $[H^0(\Omega)]^2$, in which case the norm and inner product are denoted by $(\cdot,\cdot)$ and $\|\cdot\|$, respectively. As usual, $H_0^k(\Omega)$ denotes the closure of $C_0^\infty(\Omega)$ with respect to the norm $\|\cdot\|_k$. See [10] for more detail.

We apply operators to the 2-vector function

$$\mathbf{u} = \begin{pmatrix} u_1 \\ u_2 \end{pmatrix}$$

componentwise. For example,

$$\nabla\mathbf{u} = \begin{pmatrix} \nabla u_1 \\ \nabla u_2 \end{pmatrix}.$$

If $\mathbf{U}_1$ and $\mathbf{U}_2$ are 2-vector functions, then we write the block column vector

$$\mathbf{U} \equiv \begin{pmatrix} \mathbf{U}_1 \\ \mathbf{U}_2 \end{pmatrix}.$$

If D is an operator on 2-vector functions (e.g., $D=\nabla\cdot$, $\nabla\times$, or $\boldsymbol{\tau}\cdot$), then its extension to block column vectors is defined by

$$D\mathbf{U} = \begin{pmatrix} D\mathbf{U}_1 \\ D\mathbf{U}_2 \end{pmatrix}.$$

Inner products and norms on column vector functions are defined in the natural componentwise way: $\|\mathbf{U}\|^2 = \sum_{i=1}^2 \|\mathbf{U}_i\|^2$. We introduce the *displacement flux* variable $\mathbf{U} = \nabla\mathbf{u}$:

$$\mathbf{U} = (U_1, U_2, U_3, U_4)^t = (\partial_1 u_1, \partial_2 u_1, \partial_1 u_2, \partial_2 u_2)^t.$$

2.1. Pure traction: $\boldsymbol{\Gamma_D = \emptyset}$. Let $\mathcal{N}$ denote the space of infinitesimal rigid motions:

$$\mathcal{N} := \left\{ \mathbf{u} : \mathbf{u} = \begin{pmatrix} a + bx_2 \\ c - bx_1 \end{pmatrix}, \quad a,b,c \in \mathbb{R} \right\}.$$

Let $\mathcal{N}^\perp$ be its orthogonal complement in $[L^2(\Omega)]^2$ and $\mathcal{N}^c$ its orthogonal complement in $[H^1(\Omega)]^2$. Then $\mathbf{u} \in \mathcal{N}^c$ if and only if

$$\int_\Omega \mathbf{u}\, dx = \mathbf{0}, \tag{2}$$

$$\int_\Omega \nabla \times \mathbf{u}\, dx = 0, \tag{3}$$

where $\nabla \times \mathbf{u} := \partial_1 u_2 - \partial_2 u_1$. For uniqueness of solution of pure traction problem (1), we impose the restriction that $\mathbf{u} \in \mathcal{N}^c$. For a solution of (1) to exist, the source term $\mathbf{f} \in [L^2(\Omega)]^2$ must satisfy the compatibility condition

$$\int_\Omega \mathbf{f} \cdot \mathbf{v}\, dx = 0 \quad \forall \mathbf{v} \in \mathcal{N};$$

i.e., we must have $\mathbf{f} \in \mathcal{N}^{\perp}$. (See [2, 12] for more detail.) We assume this compatibility condition to hold in what follows for the pure traction problem.

We set $\mu = 1$ without loss of generality. Problem (1) can then be rewritten in the compact form

$$\begin{aligned} -\nabla \cdot (A\nabla \mathbf{u}) &= \mathbf{f} \quad \text{in} \quad \Omega\,, \\ \mathbf{n} \cdot (A\nabla \mathbf{u}) &= \mathbf{0} \quad \text{on} \quad \Gamma\,, \end{aligned} \tag{4}$$

where

$$A = \begin{pmatrix} \lambda+2 & 0 & 0 & \lambda \\ 0 & 1 & 1 & 0 \\ 0 & 1 & 1 & 0 \\ \lambda & 0 & 0 & \lambda+2 \end{pmatrix}.$$

Since the definition of $\mathbf{U}$ implies that $\nabla \times \mathbf{U} = \mathbf{0}$ in Ω, then a system that is equivalent to (4) is

$$\begin{aligned} \mathbf{U} - \nabla \mathbf{u} &= \mathbf{0} \quad \text{in} \quad \Omega\,, \\ -\nabla \cdot A\mathbf{U} &= \mathbf{f} \quad \text{in} \quad \Omega\,, \\ \nabla \times \mathbf{U} &= \mathbf{0} \quad \text{in} \quad \Omega\,, \\ \mathbf{n} \cdot A\mathbf{U} &= \mathbf{0} \quad \text{on} \quad \Gamma\,. \end{aligned}$$

What is perhaps more important than this extended system in practice is the so-called *first-stage* system that involves $\mathbf{U}$ only:

$$\begin{aligned} -\nabla \cdot A\mathbf{U} &= \mathbf{f} \quad \text{in} \quad \Omega\,, \\ \nabla \times \mathbf{U} &= \mathbf{0} \quad \text{in} \quad \Omega\,, \\ \mathbf{n} \cdot A\mathbf{U} &= \mathbf{0} \quad \text{on} \quad \Gamma\,. \end{aligned} \tag{5}$$

It is shown in [8] that this reduced system is well posed. Note that an approximate displacement $\mathbf{u}$ can be found once $\mathbf{U}$ has been computed by solving the *second-stage* system

$$\begin{aligned} \nabla \mathbf{u} &= \mathbf{U} \quad \text{in} \quad \Omega\,, \\ \mathbf{n} \cdot A\nabla \mathbf{u} &= \mathbf{0} \quad \text{on} \quad \Gamma\,. \end{aligned}$$

See [8] for details.

We define a solution space for the primitive variables by

$$\mathcal{W} = \{\mathbf{u} \in \mathcal{N}^c : \nabla \cdot (A\nabla \mathbf{u}) \in [L^2(\Omega)]^2, \mathbf{n} \cdot (A\nabla \mathbf{u}) = \mathbf{0} \text{ on } \Gamma\}\,.$$

Since we have posed (4) on the space $\mathcal{W}$, then (3) implies that

$$\int_{\Omega} (U_2 - U_3)\, dx = 0, \quad \text{i.e.,} \quad \mathbf{U} \perp (0, 1, -1, 0)^t\,.$$

We thus define the solution space for the new variables by

$$\mathcal{V}_T = \{\mathbf{U} \in [H^1(\Omega)]^4 : \mathbf{n} \cdot A\mathbf{U} = \mathbf{0} \text{ on } \Gamma, \mathbf{U} \perp (0, 1, -1, 0)^t\}\,.$$

2.2. Pure displacement: $\boldsymbol{\Gamma_T = \emptyset}$. With $\mu = 1$, problem (1) can be rewritten in the compact form

$$\begin{aligned} -\nabla \cdot (A\nabla \mathbf{u}) &= \mathbf{f} \quad \text{in} \quad \Omega\,, \\ \mathbf{u} &= \mathbf{0} \quad \text{on} \quad \Gamma\,. \end{aligned}$$

The corresponding first-stage system is

$$\begin{aligned} -\nabla \cdot A\mathbf{U} &= \mathbf{f} \quad \text{in} \quad \Omega\,, \\ \nabla \times \mathbf{U} &= \mathbf{0} \quad \text{in} \quad \Omega\,, \\ \boldsymbol{\tau} \cdot \mathbf{U} &= \mathbf{0} \quad \text{on} \quad \Gamma\,, \end{aligned} \tag{6}$$

where $\boldsymbol{\tau} = (\tau_1, \tau_2)^t$ denotes the counterclockwise-oriented unit tangent vector on the boundary.

Since the boundary conditions of the pure displacement problem are different from those of the pure traction problem, we have a different solution space for the primitive variables:

$$\mathcal{W} = \{\mathbf{u} \in [H_0^2(\Omega)]^2 : \nabla \cdot (A\nabla \mathbf{u}) \in [L^2(\Omega)]^2\}\,.$$

The corresponding solution space for the new variables is thus

$$\mathcal{V}_D = \{\mathbf{U} \in [H^1(\Omega)]^4 : \boldsymbol{\tau} \cdot \mathbf{U} = \mathbf{0} \text{ on } \Gamma\}\,.$$

2.3. Mixed boundary conditions: $\boldsymbol{|\Gamma_T| > 0, |\Gamma_D| > 0}$. With $\mu = 1$, the first-stage system for problem (1) is

$$\begin{aligned} -\nabla \cdot A\mathbf{U} &= \mathbf{f} \quad \text{in} \quad \Omega\,, \\ \nabla \times \mathbf{U} &= \mathbf{0} \quad \text{in} \quad \Omega\,, \\ \mathbf{n} \cdot A\mathbf{U} &= \mathbf{0} \quad \text{on} \quad \Gamma_T\,, \\ \boldsymbol{\tau} \cdot \mathbf{U} &= \mathbf{0} \quad \text{on} \quad \Gamma_D\,, \end{aligned} \tag{7}$$

with corresponding solution space

$$\mathcal{V}_M = \{\mathbf{U} \in [H^1(\Omega)]^4 : \mathbf{n} \cdot A\mathbf{U} = \mathbf{0} \text{ on } \Gamma_T, \boldsymbol{\tau} \cdot \mathbf{U} = \mathbf{0} \text{ on } \Gamma_D\}\,.$$

3. First-order system least squares. Here we introduce two different approaches for solving (5), (6), and (7). The first involves applying FOSLS directly to (5). The second comes from applying FOSLS to a generalized Stokes equation. Here we describe only the FOSLS formulations for solving (5), since (6) and (7) are the same up to boundary conditions.

3.1. Direct approach. Define

$$G_0(\mathbf{U}; \mathbf{f}) = \|\mathbf{f} + \nabla \cdot A\mathbf{U}\|^2 + \|\nabla \times \mathbf{U}\|^2 \quad \text{for } \mathbf{U} \in \mathcal{V}_T\,.$$

Consider the rotation determined by the matrix

$$Q = \begin{pmatrix} \frac{1}{\sqrt{2}} & 0 & 0 & \frac{1}{\sqrt{2}} \\ 0 & 1 & 0 & 0 \\ 0 & 0 & 1 & 0 \\ \frac{1}{\sqrt{2}} & 0 & 0 & -\frac{1}{\sqrt{2}} \end{pmatrix},$$

and define the space $\tilde{\mathcal{V}} \equiv Q\mathcal{V}_T = \{\mathbf{V} = Q\mathbf{U} : \mathbf{U} \in \mathcal{V}_T\}$. Note that $\mathcal{V}_T = Q\tilde{\mathcal{V}}$ and that each vector $\mathbf{U} \in \mathcal{V}_T$ is of the form $\mathbf{U} = Q\mathbf{V}$, for some $\mathbf{V} \in \tilde{\mathcal{V}}$.

The solution $\mathbf{U} = Q\mathbf{V}$ of reduced system (5) can be obtained from the solution of the following "direct" minimization problem:

$$\mathbf{V} = \operatorname{argmin}\{G_0(Q\mathbf{W};\mathbf{f}) : \mathbf{W} \in [H^1(\Omega)]^4, \mathbf{n}\cdot AQ\mathbf{W} = \mathbf{0} \text{ on } \Gamma, \mathbf{W} \perp (0,1,-1,0)^t\}\,.$$

Consider the scaling determined by the matrix

$$D = \begin{pmatrix} \frac{1}{\lambda} & 0 & 0 & 0 \\ 0 & 1 & 0 & 0 \\ 0 & 0 & 1 & 0 \\ 0 & 0 & 0 & 1 \end{pmatrix}.$$

Now let $\mathbf{V} = D^{-1}Q\mathbf{U}$ and

$$B = AQD = \begin{pmatrix} \sqrt{2}(1+\frac{1}{\lambda}) & 0 & 0 & \sqrt{2} \\ 0 & 1 & 1 & 0 \\ 0 & 1 & 1 & 0 \\ \sqrt{2}(1+\frac{1}{\lambda}) & 0 & 0 & -\sqrt{2} \end{pmatrix}.$$

Note that $\mathbf{U} = QD\mathbf{V}$. We thus have that $\nabla\cdot A\mathbf{U} = \nabla\cdot B\mathbf{V}$ and $\nabla\times\mathbf{U} = \nabla\times QD\mathbf{V}$. Our modified problem is therefore given by

$$\mathbf{V} = \operatorname{argmin}\{G_1(\mathbf{W};\mathbf{f}) : \mathbf{W} \in [H^1(\Omega)]^4, \mathbf{n}\cdot B\mathbf{W} = \mathbf{0} \text{ on } \Gamma, \mathbf{W} \perp (0,1,-1,0)^t\}\,, \tag{8}$$

where

$$G_1(\mathbf{W};\mathbf{f}) = \|\mathbf{f} + \nabla\cdot B\mathbf{W}\|^2 + \|\nabla\times QD\mathbf{W}\|^2 \quad \text{for } \mathbf{W} \in D^{-1}Q\mathcal{V}_T\,.$$

3.2. Stokes approach. Consider the operators

$$\nabla\cdot A = \begin{pmatrix} (\lambda+2)\partial_1 & \partial_2 & \partial_2 & \lambda\partial_1 \\ \lambda\partial_2 & \partial_1 & \partial_1 & (\lambda+2)\partial_2 \end{pmatrix}, \tag{9}$$

$$\nabla\times = \begin{pmatrix} \partial_2 & -\partial_1 & 0 & 0 \\ 0 & 0 & \partial_2 & -\partial_1 \end{pmatrix}.$$

If we first subtract row 2 of $\nabla\times$ from row 1 of $\nabla\cdot A$, then add row 1 of $\nabla\times$ to row 2 of $\nabla\cdot A$, but leave $\nabla\times$ alone, then we obtain the operators

$$\nabla\cdot A_s = \begin{pmatrix} (\lambda+2)\partial_1 & \partial_2 & 0 & (\lambda+1)\partial_1 \\ (\lambda+1)\partial_2 & 0 & \partial_1 & (\lambda+2)\partial_2 \end{pmatrix}, \tag{10}$$

$$\nabla\cdot B_s = \nabla\cdot A_sQD = \begin{pmatrix} \frac{2\lambda+3}{\sqrt{2}\lambda}\partial_1 & \partial_2 & 0 & \frac{1}{\sqrt{2}}\partial_1 \\ \frac{2\lambda+3}{\sqrt{2}\lambda}\partial_2 & 0 & \partial_1 & -\frac{1}{\sqrt{2}}\partial_2 \end{pmatrix},$$

$$\nabla\times QD = \begin{pmatrix} \frac{1}{\sqrt{2}\lambda}\partial_2 & -\partial_1 & 0 & \frac{1}{\sqrt{2}}\partial_2 \\ -\frac{1}{\sqrt{2}\lambda}\partial_1 & 0 & \partial_2 & \frac{1}{\sqrt{2}}\partial_1 \end{pmatrix}.$$

This leads to the "Stokes" minimization problem given by

$$\mathbf{V} = \operatorname{argmin}\{G_2(\mathbf{W};\mathbf{f}) : \mathbf{W} \in [H^1(\Omega)]^4, \mathbf{n}\cdot B\mathbf{W} = \mathbf{0} \text{ on } \Gamma, \mathbf{W} \perp (0,1,-1,0)^t\}\,, \tag{11}$$

where

$$G_2(\mathbf{W};\mathbf{f}) = \|\mathbf{f} + \nabla \cdot B_s\mathbf{W}\|^2 + \|\nabla \times QD\mathbf{W}\|^2 \quad \text{for } \mathbf{W} \in D^{-1}Q\mathcal{V}_T\,.$$

Note that the source term and the boundary conditions for (11) are the same as those for (8).

These two approaches apply to (6) and (7) simply by redefining the underlying space appropriately.

4. Numerical methods. We now turn to numerical methods for approximating the solution $\mathbf{V}$ of (8) and (11).

4.1. Finite elements. Domain Ω is subdivided into a set $\mathcal{T}_h$ of nonoverlapping rectangles such that $\Omega = \cup_{T\in\mathcal{T}_h} T$ and no vertex of one rectangle lies on the edge of another. Here, $h := \max_{T\in\mathcal{T}_h} \operatorname{diam} T$. The refined set $\mathcal{T}_{h/2}$ is obtained by connecting the midpoints of the opposite edges of the rectangles in $\mathcal{T}_h$. Define the finite element space

$$\begin{aligned}\mathcal{V}_h := \{\mathbf{U} : \mathbf{U}|_T \text{ is bilinear } \forall\ T \in \mathcal{T}_h, \mathbf{U} \text{ is continuous on } \Omega,\\ \mathbf{n}\cdot A\mathbf{U} = \mathbf{0} \text{ on } \Gamma\,, \mathbf{U} \perp (0,1,-1,0)^t\,\}.\end{aligned}$$

Note that $\mathcal{V}_h \subset \mathcal{V}_{h/2} \subset [H^1(\Omega)]^4$. Then the following approximation property holds: there exists a constant C such that, for all $\mathbf{V} \in \mathcal{V}_T$, there exists $\mathbf{V}_h \in \mathcal{V}_h$ such that

$$\|V_j - V_{j\,h}\| + h\|V_j - V_{j\,h}\|_1 \le Ch^2\|V_j\|_2, \qquad j = 1,\ldots,4\,.$$

4.2. Multigrid (MG). The multigrid (MG) algorithm adopted in this paper is most easily described in the present context as a functional minimization process. Here we describe a simple two-level procedure that provides the basis for V, W, and full multigrid (FMG) cycle algorithms in the usual way. See [5] for more detail on MG methods.

Suppose we are given a current approximation $\mathbf{V}_h \in \mathcal{V}_h$ to the solution of the minimization problem

$$\mathbf{V} = \operatorname{argmin}\{G(\mathbf{W};\mathbf{f}) : \mathbf{W} \in \mathcal{V}\}\,. \tag{12}$$

Here, $G = G_1$ or G_2 and the minimization is to be taken over the corresponding subspace $\mathcal{V}$ of $[H^1(\Omega)]^4$ with appropriate boundary conditions. Then the MG on level h consists of the following two steps (h_0 represents the coarsest grid):

Relaxation. If $h = h_0$, then define $\mathbf{V}_h \in \mathcal{V}_h$ to be the exact solution of

$$\mathbf{V}_h = \operatorname{argmin}\{G(\mathbf{W}_h;\mathbf{f}) : \mathbf{W}_h \in \mathcal{V}_h\}\,.$$

If $h < h_0$, then perform one nodal block Gauss–Seidel relaxation sweep as follows: Let n_h denote the number of nodes on level h including boundary nodes and, for each $l \in \{1,2,\ldots,n_h\}$, let $\mathcal{V}_h^l$ denote the subspace of $\mathcal{V}_h$ of vector functions $\mathbf{W}_h^l$ that are zero at all nodes except node l; then one relaxation sweep is as follows:

For $l = 1,2,\ldots,n_h$ in turn,

let $\mathbf{V}_h^l \in \mathcal{V}_h^l$ solve

$$\mathbf{V}_h^l = \text{argmin}\{G(\mathbf{V}_h + \mathbf{W}_h^l; \mathbf{f}) : \mathbf{W}_h^l \in \mathcal{V}_h^l\}$$

and set $\mathbf{V}_h \leftarrow \mathbf{V}_h + \mathbf{V}_h^l$.

Coarsening. If $h < h_0$,

let $\mathbf{V}_{2h} \in \mathcal{V}_{2h}$ solve

$$\mathbf{V}_{2h} = \text{argmin}\{G(\mathbf{V}_h + \mathbf{W}_{2h}; \mathbf{f}) : \mathbf{W}_{2h} \in \mathcal{V}_{2h}\}$$

and set $\mathbf{V}_h \leftarrow \mathbf{V}_h + \mathbf{V}_{2h}$.

The relaxation described above is not strictly well-defined: we cannot generally change $\mathbf{V}$'s second and third components, V_2 and V_3, at a node and expect the new approximation to be in the space $\mathcal{V}$, that is, nodal relaxation will tend to violate the condition $\mathbf{V} \perp (0, 1, -1, 0)^t$. (On level $h = h_0$, this is not a concern because we simply solve the minimization problem with this added constraint, which guarantees a unique solution.) The relaxation process we use actually suspends this condition during a given sweep of the grid points, but imposes it on the approximation obtained after each sweep by invoking the Gram–Schmidt step

$$\begin{pmatrix} V_2 \\ V_3 \end{pmatrix} \leftarrow \begin{pmatrix} V_2 \\ V_3 \end{pmatrix} - \frac{\int_\Omega (V_2 - V_3)\, dx}{2 \int_\Omega dx} \begin{pmatrix} 1 \\ -1 \end{pmatrix}.$$

(This Gram–Schmidt step is neither necessary nor appropriate for the pure displacement or the mixed boundary value problem.)

This two-grid scheme is the basis for the more practical cycling scheme that we use here. Our tests focus on $\mathsf{V}(\nu_1, \nu_2)$ cycles, which use $\nu_1 \geq 0$ relaxation sweeps before coarsening, one recursive solve of the coarse grid equations (that is, one application of a $\mathsf{V}(\nu_1, \nu_2)$ cycle to solve the coarse grid equations), and $\nu_2 \geq 0$ relaxation sweeps after coarsening. We also use $\mathsf{W}(\nu_1, \nu_2)$ cycles, which are similar except that they involve two recursive solves on the coarse grid. Finally, we will also consider the full multigrid scheme FMG($n\mathsf{V}(\nu_1, \nu_2)$), which proceeds from the coarsest to the finest grid, invoking $n \geq 1$ $\mathsf{V}(\nu_1, \nu_2)$ cycles on each level along the way. Thus, each coarse level serves to provide a good initial approximation to the next finer level, with the intent of producing a final approximation on the finest grid that is accurate to the level of discretization error. This FMG($n\mathsf{V}(\nu_1, \nu_2)$) cycle scheme is described abstractly as follows:

(1) Solve the level $h = h_0$ problem exactly.
(2) For $h = h_0, h_0/2, \ldots$ until the finest level is reached, interpolate the level h approximation to level $h/2$ to act as an initial guess and perform n $\mathsf{V}(\nu_1, \nu_2)$ cycles on level $h/2$.

FMG($n\mathsf{W}(\nu_1, \nu_2)$) cycles are defined analogously.

5. Numerical results. In this section, we begin by studying the pure traction problem. MG solver performance and finite element discretization accuracy are first analyzed individually, then overall FMG performance is assessed. We then continue this study with the pure displacement and mixed problems. The pure traction problem V cycle results show that our approach achieves optimal λ-uniform performance that is essentially what we expect from applying MG to well-behaved Poisson equations. The pure displacement and mixed problems exhibit less satisfactory results,

TABLE 1
Convergence factors for $V(1,0)$ based on G_1 for the pure traction problem.

	$h=\frac{1}{4}$	$h=\frac{1}{8}$	$h=\frac{1}{16}$	$h=\frac{1}{32}$
$\lambda=10$	0.5769	0.7604	0.8024	0.8142
$\lambda=100$	0.5887	0.7871	0.8263	0.8353
$\lambda=1000$	0.5904	0.7899	0.8288	0.8375

TABLE 2
Convergence factors for $V(1,1)$ based on G_1 for the pure traction problem.

	$h=\frac{1}{4}$	$h=\frac{1}{8}$	$h=\frac{1}{16}$	$h=\frac{1}{32}$
$\lambda=10$	0.3521	0.5830	0.6333	0.6706
$\lambda=100$	0.3722	0.6225	0.6800	0.7096
$\lambda=1000$	0.3754	0.6268	0.6849	0.7138

TABLE 3
Convergence factors for $V(2,1)$ based on G_1 for the pure traction problem.

	$h=\frac{1}{4}$	$h=\frac{1}{8}$	$h=\frac{1}{16}$	$h=\frac{1}{32}$
$\lambda=10$	0.2153	0.4542	0.5049	0.5563
$\lambda=100$	0.1999	0.4987	0.5587	0.6047
$\lambda=1000$	0.1993	0.5036	0.5647	0.6100

TABLE 4
Convergence factors for $W(1,0)$ based on G_1 for the pure traction problem.

	$h=\frac{1}{4}$	$h=\frac{1}{8}$	$h=\frac{1}{16}$	$h=\frac{1}{32}$
$\lambda=10$	0.5769	0.7603	0.7982	0.8151
$\lambda=100$	0.5887	0.7878	0.8220	0.8356
$\lambda=1000$	0.5904	0.7908	0.8246	0.8377

primarily because W cycles were required to ensure effective MG and FMG performance. Nevertheless, we have obtained optimal λ-uniform performance for these cases that represents substantial improvement over other approaches (cf. [2]).

5.1. Pure traction: MG performance. To study MG performance, we begin with the homogeneous pure traction model problem with $\mu = 1$:

$$-\Delta\mathbf{u} - (\lambda+1)\nabla\nabla\cdot\mathbf{u} = \mathbf{0} \quad \text{in} \quad \Omega = [0,1]^2\,,$$
$$\sum_{j=1}^{2}\sigma_{ij}(\mathbf{u})n_j = 0 \quad \text{on} \quad \Gamma, \quad 1 \le i \le 2\,.$$

For concreteness, let the east, west, south, and north boundaries of Γ be denoted by Γ_E, Γ_W, Γ_S, and Γ_N, respectively. The boundary conditions for the unit square are

$$V_2 + V_3 = 0 \quad \text{on} \quad \Gamma\,,$$
$$\left(1+\frac{1}{\lambda}\right)V_1 + V_4 = 0 \quad \text{on} \quad \Gamma_E \cup \Gamma_W\,,$$

TABLE 5
Convergence factors for $\mathsf{V}(1,0)$ based on G_2 for the pure traction problem.

	$h=\frac{1}{4}$	$h=\frac{1}{8}$	$h=\frac{1}{16}$	$h=\frac{1}{32}$
$\lambda=10$	0.5175	0.5425	0.6173	0.6400
$\lambda=100$	0.5198	0.5492	0.6110	0.6402
$\lambda=1000$	0.5201	0.5512	0.6124	0.6416

TABLE 6
Convergence factors for $\mathsf{V}(1,1)$ based on G_2 for the pure traction problem.

	$h=\frac{1}{4}$	$h=\frac{1}{8}$	$h=\frac{1}{16}$	$h=\frac{1}{32}$
$\lambda=10$	0.3500	0.4501	0.4893	0.5134
$\lambda=100$	0.3413	0.4237	0.4727	0.5083
$\lambda=1000$	0.3403	0.4222	0.4717	0.5081

TABLE 7
Convergence factors for $\mathsf{V}(2,1)$ based on G_2 for the pure traction problem.

	$h=\frac{1}{4}$	$h=\frac{1}{8}$	$h=\frac{1}{16}$	$h=\frac{1}{32}$
$\lambda=10$	0.2536	0.3829	0.4223	0.4442
$\lambda=100$	0.2405	0.3576	0.3902	0.4289
$\lambda=1000$	0.2491	0.3520	0.3866	0.4278

TABLE 8
Convergence factors for $\mathsf{W}(1,0)$ based on G_2 for the pure traction problem.

	$h=\frac{1}{4}$	$h=\frac{1}{8}$	$h=\frac{1}{16}$	$h=\frac{1}{32}$
$\lambda=10$	0.5175	0.4944	0.5710	0.6070
$\lambda=100$	0.5198	0.5263	0.6019	0.6344
$\lambda=1000$	0.5201	0.5300	0.6054	0.6376

$$\left(1+\frac{1}{\lambda}\right)V_1 - V_4 = 0 \quad \text{on} \quad \Gamma_N \cup \Gamma_S\,.$$

Of course, the exact solution is zero, but this allows us to study asymptotic MG convergence factors without concern for the limits of floating-point arithmetic. For this purpose, we use random initial guesses. The discretization uses uniform grids. The experiments reported here were run in double-precision arithmetic on a SUN Ultra-2 Workstation.

We assess MG efficiency here by measuring the convergence factors as ratios of successive square roots of functional values $G_i(\mathbf{V};0)$ $(i=1,2)$. This measure is appropriate because it estimates the worst-case factor in the norm induced by the functional, which is the asymptotic convergence factor in any discrete (and therefore equivalent) matrix norm.

Tables 1 through 4 depict convergence factors measured after 20 multigrid cycles based on the functional G_1 in (8). Numerical results show that the more expensive W cycle does not give better factors than the V cycle. This suggests that MG perfor-

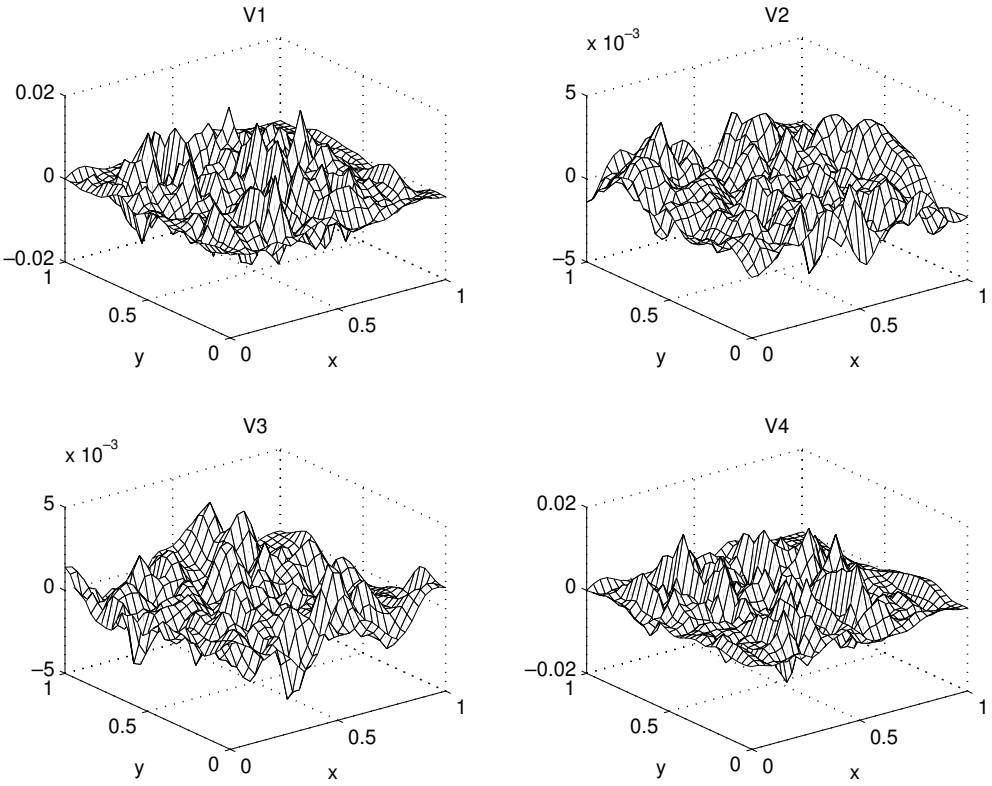

FIG. 1. *Errors after* 20 $V(1,0)$ *cycles based on* G_1 *for the pure traction problem.*

mance is limited by the connections between variables that is at least as strong in the oscillatory components as it is in the smooth ones. This can be confirmed by model problem analysis.

Tables 5 through 8 represent convergence factors measured after 20 multigrid cycles based on the functional G_2 in (11). Note that these factors for the Stokes approach are generally better than those for the direct approach. In fact, operator (10) is derived from (9) by two elementary row operations that simplify the coupling between V_2 and V_3, so the superiority of the Stokes approach is not surprising. Note also that the W cycle again provides no improvement. The numerical results reported here seem to confirm the theoretical assertion that both MG methods converge with factors that are bounded independent of λ.

5.2. Pure traction: Improved MG ($\mathbf{V}^+$). Figures 1 and 2 represent the errors after 20 V(1,0) cycles for $h = \frac{1}{32}$ and $\lambda = 1000$. Figure 1 shows that the multigrid method for FOSLS based on G_1 produces errors that have both smooth and oscillatory components, while Figure 2 shows that the multigrid method for FOSLS based on G_2 produces errors that have predominantly smooth components. Figure 2 also shows that errors for the standard MG scheme applied to G_2 are concentrated at the boundary. To capitalize on this concentration, we modified MG by including one nodal block Gauss–Seidel iteration on the boundary after each standard smoothing iteration. We regard this pair of smoothing steps as one smoothing iteration; the additional computational cost is not significant when the size of the problem is large

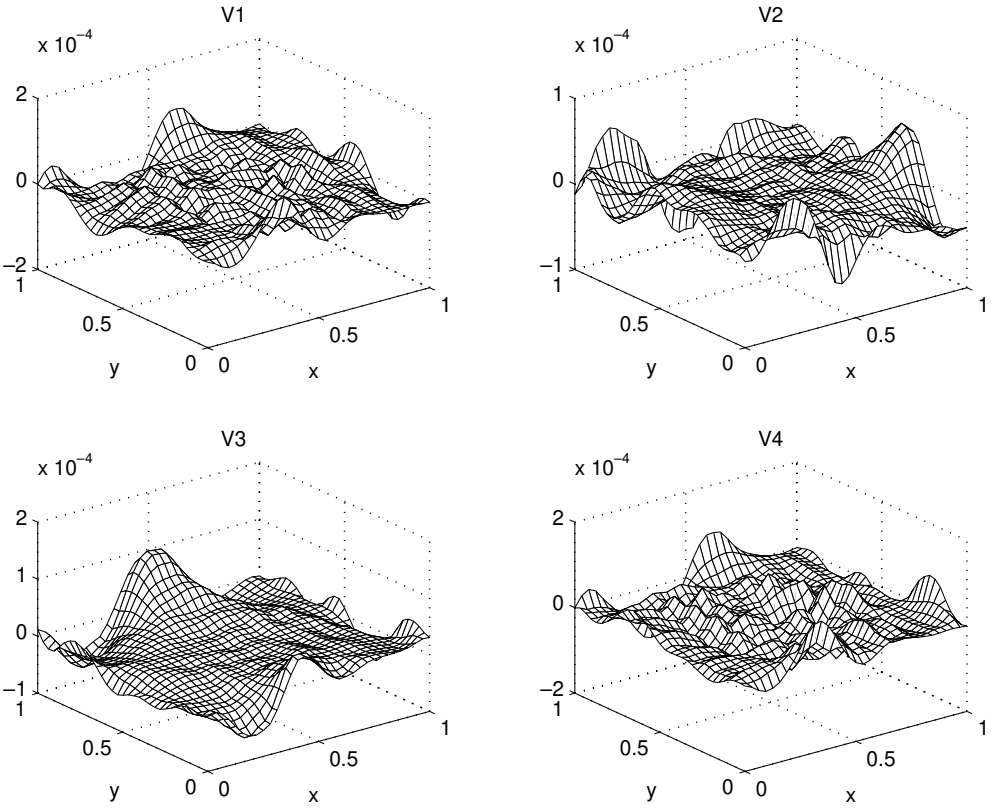

FIG. 2. *Errors after* 20 $V(1,0)$ *cycles based on* G_2 *for the pure traction problem.*

because the boundary is a proportionately small fraction of the grid. We denote the corresponding V cycle algorithm by V^+. Tables 9–11 depict the V^+ cycle convergence factors, and Figure 3 represents errors after 20 $\mathsf{V}(1,0)^+$ cycles for $h = \frac{1}{32}$ and $\lambda = 1000$.

The observed convergence factors and shape and magnitude of the errors suggest that V^+ based on G_2 might be the method of choice for large-scale problems. A $\mathsf{V}(1,1)^+$ cycle costs about 50% more than a $\mathsf{V}(1,0)^+$ cycle, and a $\mathsf{V}(2,1)^+$ cycle costs about twice as much. This suggests that the $\mathsf{V}(1,1)^+$ algorithm based on G_2 is the most effective solver.

5.3. Pure traction: Discretization errors and FMG performance. To measure discretization error, we constructed a problem with a known nonzero solution. Let the domain Ω be the unit square. The function

$$\mathbf{u} = \begin{pmatrix} u_1 \\ u_2 \end{pmatrix} = \begin{pmatrix} x(1-x)y^2(1-y)^2 \sin \pi x - \frac{2}{15\pi^3} \\ x^2(1-x)^2 y^2(1-y)^2 \cos \pi y \end{pmatrix}$$

satisfies the pure traction boundary condition in (1) and compatibility conditions (2) and (3). Regarding $\mathbf{u}$ as the displacement solution of (1), we obtained the exact $\mathbf{V} = D^{-1}Q\nabla\mathbf{u}$ and $\mathbf{f} = -\nabla \cdot A\nabla\mathbf{u}$. (Note that the solutions here are very smooth: $\mathbf{u} \in [H^3(\Omega)]^2$ and $\mathbf{V} \in [H^2(\Omega)]^4$.) With this $\mathbf{f}$, we used many V^+ cycles to find the approximate solution of (11) on each of the various levels of discretization. (We used 20 $\mathsf{V}(1,1)^+$ cycles in this case to ensure that the errors properly reflected discretization accuracy, without contamination from algebraic iteration errors.)

TABLE 9
Convergence factors for $\mathsf{V}(1,0)^+$ based on G_2 for the pure traction problem.

	$h=\frac{1}{4}$	$h=\frac{1}{8}$	$h=\frac{1}{16}$	$h=\frac{1}{32}$
$\lambda=10$	0.4664	0.4970	0.5639	0.6046
$\lambda=100$	0.4677	0.5260	0.5967	0.6318
$\lambda=1000$	0.4680	0.5295	0.6005	0.6350

TABLE 10
Convergence factors for $\mathsf{V}(1,1)^+$ based on G_2 for the pure traction problem.

	$h=\frac{1}{4}$	$h=\frac{1}{8}$	$h=\frac{1}{16}$	$h=\frac{1}{32}$
$\lambda=10$	0.2524	0.3783	0.4205	0.4439
$\lambda=100$	0.2404	0.3503	0.3951	0.4231
$\lambda=1000$	0.2392	0.3445	0.3925	0.4214

TABLE 11
Convergence factors for $\mathsf{V}(2,1)^+$ based on G_2 for the pure traction problem.

	$h=\frac{1}{4}$	$h=\frac{1}{8}$	$h=\frac{1}{16}$	$h=\frac{1}{32}$
$\lambda=10$	0.1697	0.2975	0.3148	0.3694
$\lambda=100$	0.1567	0.2800	0.3060	0.3546
$\lambda=1000$	0.1553	0.2781	0.3058	0.3539

Tables 12 and 13 show that the relative discretization errors are $O(h^2)$ with respect to both L^2 and G_2 functional norms ($G_2^{1/2}$). The functional norms are appropriate here for measuring discretization error (and below for measuring FMG performance) because they are equivalent to the H^1 norm. The theoretically predicted error bounds are $O(h^2)$ in L^2 but only $O(h)$ in $G_2^{1/2}$. We therefore appear to have obtained superconvergence for this particular case, just as was observed for the least-squares treatment of the Helmholtz equation in [9].

To test overall accuracy for FMG, we studied FMG based on 3 $\mathsf{V}(1,1)^+$ cycles. Tables 14 and 15 show that FMG(3$\mathsf{V}(1,1)^+$) produces a total error (i.e., the L^2 or functional norm of the difference of the computed and exact solution of (1)) that compares favorably to the discretization errors estimated in Tables 12 and 13. This implies that the problem on level h can be solved to within the level of discretization error at a cost of about $4/3 \cdot 3\mathsf{V}(1,1)^+ = 4\ \mathsf{V}(1,1)^+$ cycles on level h, regardless of the size of λ.

5.4. Pure displacement: MG performance. To measure MG performance, we again take $\mathbf{f}=\mathbf{0}$ and $\mu=1$ in problem (1). The Dirichlet boundary conditions for the displacement variables become tangential boundary conditions for the flux variables $\mathbf{V}$. This leads to the "Stokes" minimization problem given by

$$\mathbf{V} = \operatorname{argmin}\{G_2(\mathbf{W};\mathbf{f}) : \mathbf{W} \in [H^1(\Omega)]^4, \boldsymbol{\tau}\cdot QD\mathbf{W} = 0 \text{ on } \Gamma\}\,. \tag{13}$$

For the unit square, the boundary conditions in (13) are

$$\frac{1}{\lambda}V_1 - V_4 = 0, \quad V_2 = 0 \quad \text{on} \quad \Gamma_E \cup \Gamma_W\,, \tag{14}$$

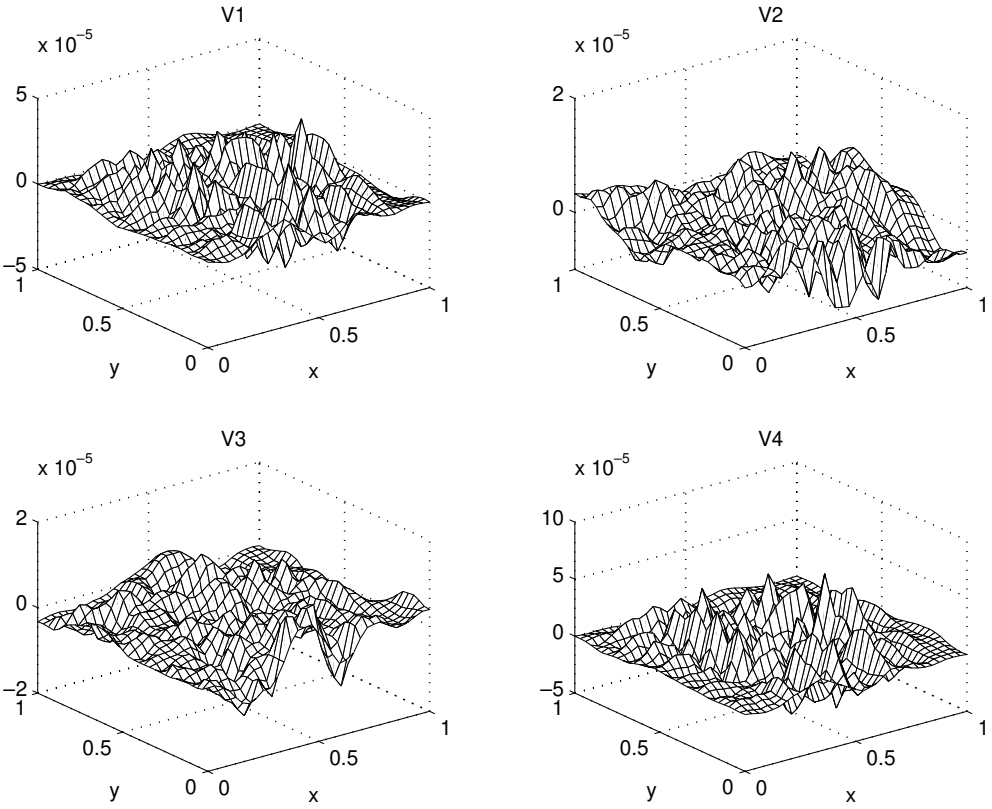

FIG. 3. *Errors after* 20 $V(1,0)^+$ *cycles based on* G_2 *for the pure traction problem.*

TABLE 12
Discretization errors in the L^2 *norm and their convergence factors for the pure traction problem.*

	$\lambda = 10$		$\lambda = 100$		$\lambda = 1000$	
	L^2 norm	factor	L^2 norm	factor	L^2 norm	factor
$h = 1/4$	0.5170		0.4115		0.4011	
$h = 1/8$	0.1295	0.2505	9.871E-2	0.2399	9.581E-2	0.2389
$h = 1/16$	3.103E-2	0.2396	2.337E-2	0.2368	2.267E-2	0.2366
$h = 1/32$	7.337E-3	0.2364	5.544E-3	0.2372	5.381E-3	0.2374
$h = 1/64$	1.762E-3	0.2402	1.338E-3	0.2414	1.300E-3	0.2416

TABLE 13
Discretization errors in the G_2 *functional norm and their convergence factors for the pure traction problem.*

	$\lambda = 10$		$\lambda = 100$		$\lambda = 1000$	
	$G_2^{1/2}$	factor	$G_2^{1/2}$	factor	$G_2^{1/2}$	factor
$h = 1/4$	0.1862		0.1821		0.1817	
$h = 1/8$	4.793E-2	0.2574	4.654E-2	0.2555	4.643E-2	0.2554
$h = 1/16$	1.218E-2	0.2542	1.177E-2	0.2528	1.173E-2	0.2527
$h = 1/32$	3.069E-3	0.2519	2.956E-3	0.2512	2.946E-3	0.2512
$h = 1/64$	7.694E-4	0.2507	7.404E-4	0.2505	7.380E-4	0.2505

TABLE 14

FMG($3\mathsf{V}(1,1)^+$) L^2 *norm errors and their ratios with corresponding discretization errors for the pure traction problem.*

	$\lambda = 10$		$\lambda = 100$		$\lambda = 1000$	
	L^2 norm	ratio	L^2 norm	ratio	L^2 norm	ratio
$h = 1/4$	0.5299	1.025	0.4222	1.026	0.4116	1.026
$h = 1/8$	0.1430	1.104	0.1092	1.106	0.1060	1.106
$h = 1/16$	3.813E-2	1.229	2.857E-2	1.223	2.770E-2	1.222
$h = 1/32$	9.869E-3	1.345	7.352E-3	1.326	7.130E-3	1.325
$h = 1/64$	2.516E-3	1.428	1.872E-3	1.399	1.816E-3	1.397

TABLE 15

FMG($3\mathsf{V}(1,1)^+$) G_2 *functional norm errors and their ratios with corresponding discretization errors for the pure traction problem.*

	$\lambda = 10$		$\lambda = 100$		$\lambda = 1000$	
	$G_2^{1/2}$	ratio	$G_2^{1/2}$	ratio	$G_2^{1/2}$	ratio
$h = 1/4$	0.1869	1.004	0.1827	1.003	0.1823	1.003
$h = 1/8$	4.882E-2	1.019	4.732E-2	1.017	4.793E-2	1.032
$h = 1/16$	1.272E-2	1.044	1.218E-2	1.035	1.214E-2	1.035
$h = 1/32$	3.341E-3	1.089	3.176E-3	1.074	3.164E-3	1.074
$h = 1/64$	8.989E-4	1.168	8.633E-4	1.166	8.614E-4	1.167

$$\frac{1}{\lambda}V_1 + V_4 = 0, \quad V_3 = 0 \quad \text{on} \quad \Gamma_S \cup \Gamma_N\,.$$

The numerical results given in Tables 16 through 19 show that the MG convergence factors are independent of λ, yet they differ substantially from the patterns we observed for pure traction. The factors for the V cycles here do not settle down so nicely as h is decreased. Moreover, additional relaxations and further coarse grid work appear to be very beneficial, suggesting that MG here is limited more by coupling between smooth components that are not so well attenuated by the coarsening process. This is confirmed by Figure 4, which depicts the errors after 20 V(1,0) cycles for $h = \frac{1}{32}$ and $\lambda = 1000$. These errors are very smooth, except near the boundary. This suggests several possibilities for improving V cycle convergence, including the use of conjugate gradients as an outer iteration and special relaxation schemes to attenuate errors of the type seen here. We did test several such schemes, but we will not discuss them further here because our results did not show enough improvement over that for the simpler W(1,0) cycle. Note that W(1,0) cycle performance for pure displacement (Table 19) compares well to V(1,0) cycle performance for pure traction (Table 8). Moreover, the convergence factor for W(1,0) appears to be independent of h.

5.5. Pure displacement: Discretization errors and FMG performance. To measure the discretization error, we take the function

$$\mathbf{u} = \begin{pmatrix} u_1 \\ u_2 \end{pmatrix} = \begin{pmatrix} x(1-x)y^2(1-y)^2 \sin \pi x \\ x^2(1-x)^2y^2(1-y)^2 \cos \pi y \end{pmatrix},$$

which differs from the function in section 5.3 by a constant but satisfies the pure displacement boundary condition in (1). (Note again that the solution is very smooth.) Regarding $\mathbf{u}$ as the displacement solution of (1), we obtain the same $\mathbf{V}$ and $\mathbf{f}$ as in section 5.3. With this $\mathbf{f}$, we found the approximate solution of (13) using 40 W(1,0) cycles (comparable in convergence to 20 V(1,1)$^+$ cycles for pure traction) on various

TABLE 16
Convergence factors for $\mathsf{V}(1,0)$ based on G_2 for the pure displacement problem.

	$h=\frac{1}{4}$	$h=\frac{1}{8}$	$h=\frac{1}{16}$	$h=\frac{1}{32}$
$\lambda=10$	0.5660	0.7127	0.8229	0.8977
$\lambda=100$	0.5724	0.7331	0.8383	0.8797
$\lambda=1000$	0.5728	0.7354	0.8387	0.8767

TABLE 17
Convergence factors for $\mathsf{V}(1,1)$ based on G_2 for the pure displacement problem.

	$h=\frac{1}{4}$	$h=\frac{1}{8}$	$h=\frac{1}{16}$	$h=\frac{1}{32}$
$\lambda=10$	0.5007	0.7372	0.8338	0.8962
$\lambda=100$	0.4974	0.7408	0.8380	0.8903
$\lambda=1000$	0.4963	0.7402	0.8370	0.8877

TABLE 18
Convergence factors for V(2,1) based on G_2 for the pure displacement problem.

	$h=\frac{1}{4}$	$h=\frac{1}{8}$	$h=\frac{1}{16}$	$h=\frac{1}{32}$
$\lambda=10$	0.4665	0.7144	0.8262	0.8855
$\lambda=100$	0.4588	0.7177	0.8273	0.8773
$\lambda=1000$	0.4572	0.7172	0.8263	0.8728

TABLE 19
Convergence factors for $\mathsf{W}(1,0)$ based on G_2 for the pure displacement problem.

	$h=\frac{1}{4}$	$h=\frac{1}{8}$	$h=\frac{1}{16}$	$h=\frac{1}{32}$
$\lambda=10$	0.5660	0.6263	0.6274	0.6592
$\lambda=100$	0.5724	0.6540	0.6518	0.6675
$\lambda=1000$	0.5728	0.6569	0.6539	0.6672

levels of discretization. Tables 20 and 21 show that the relative discretization errors are also $O(h^2)$ with respect to both the L^2 and G_2 functional norms ($G_2^{1/2}$).

To test overall accuracy for FMG, we studied FMG based on 6 W(1,0) cycles (comparable in convergence to 3 $\mathsf{V}(1,1)^+$ cycles for pure traction). Tables 22 and 23 show that FMG(6W(1,0)) produces a total error comparing favorably to the discretization errors estimated in Tables 20 and 21. This implies that the problem on level h can be solved to within the level of discretization error at a cost of about $4/3 \cdot 6\mathsf{W}(1,0) = 8$ W(1,0) cycles on level h, regardless of the size of λ.

5.6. Mixed boundary conditions: MG performance. We consider a homogeneous mixed boundary value model problem with $\mu = 1$:

$$
\begin{aligned}
-\Delta\mathbf{u} - (\lambda+1)\nabla\nabla\cdot\mathbf{u} &= \mathbf{0} \quad \text{in} \quad \Omega = [0,1]^2\,,\\
\sum_{j=1}^{2} \sigma_{ij}(\mathbf{u}) n_j &= 0 \quad \text{on} \quad \Gamma_T = \Gamma_E \cup \Gamma_N, \quad 1 \le i \le 2\,,\\
\mathbf{u} &= \mathbf{0} \quad \text{on} \quad \Gamma_D = \Gamma_W \cup \Gamma_S\,.
\end{aligned}
$$

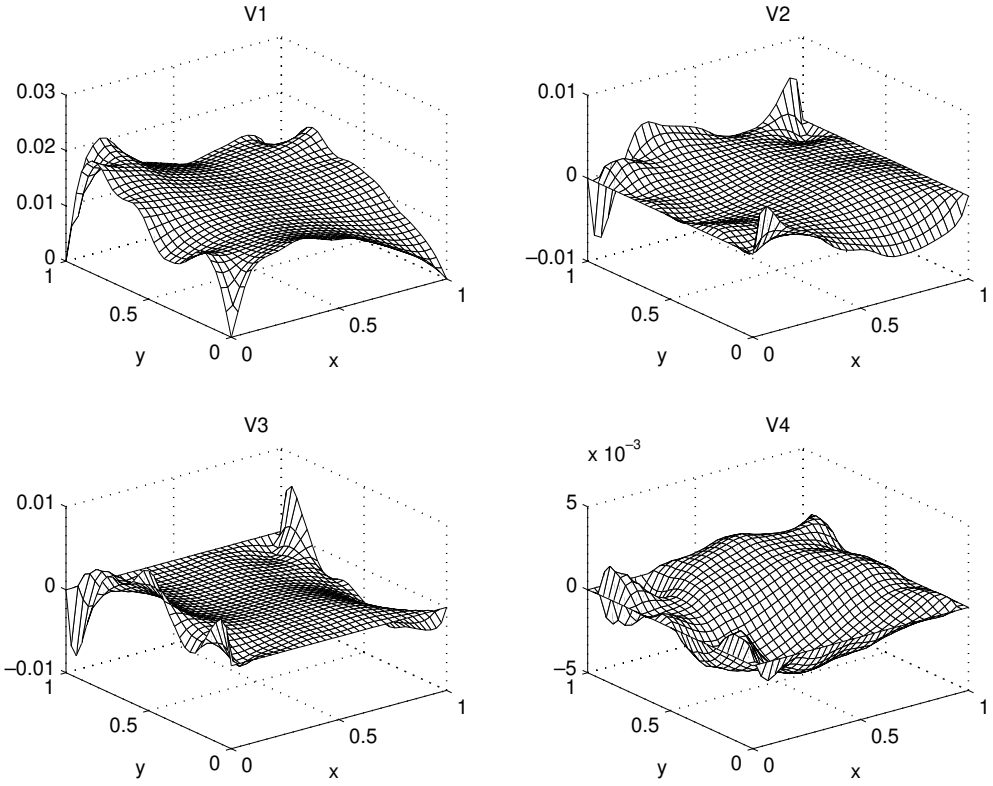

FIG. 4. *Errors after* 20 $V(1,0)$ *cycles based on* G_2 *for the pure displacement problem.*

TABLE 20

Discretization errors in the L^2 *norm and their convergence factors for the pure displacement problem.*

	$\lambda = 10$		$\lambda = 100$		$\lambda = 1000$	
	L^2 norm	factor	L^2 norm	factor	L^2 norm	factor
$h = 1/4$	0.4661		0.4292		0.4248	
$h = 1/8$	0.1181	0.2534	0.1129	0.2630	0.1122	0.2641
$h = 1/16$	2.893E-2	0.2450	2.800E-2	0.2480	2.788E-2	0.2485
$h = 1/32$	7.075E-3	0.2446	6.849E-3	0.2446	6.815E-3	0.2444
$h = 1/64$	1.743E-3	0.2464	1.682E-3	0.2456	1.672E-3	0.2453

TABLE 21

Discretization errors in the G_2 *functional norm and their convergence factors for the pure displacement problem.*

	$\lambda = 10$		$\lambda = 100$		$\lambda = 1000$	
	$G_2^{1/2}$	factor	$G_2^{1/2}$	factor	$G_2^{1/2}$	factor
$h = 1/4$	0.2051		0.2089		0.2093	
$h = 1/8$	5.127E-2	0.2500	5.268E-2	0.2522	5.285E-2	0.2525
$h = 1/16$	1.282E-2	0.2500	1.323E-2	0.2511	1.329E-2	0.2515
$h = 1/32$	3.207E-3	0.2502	3.315E-3	0.2506	3.330E-3	0.2506
$h = 1/64$	8.018E-4	0.2500	8.294E-4	0.2502	8.333E-3	0.2502

TABLE 22
FMG(6W(1,0))L^2 *norm errors and their ratios with corresponding discretization errors for the pure displacement problem.*

	$\lambda = 10$		$\lambda = 100$		$\lambda = 1000$	
	L^2 norm	ratio	L^2 norm	ratio	L^2 norm	ratio
$h = 1/4$	0.4740	1.017	0.4379	1.020	0.4336	1.021
$h = 1/8$	0.1228	1.040	0.1181	1.046	0.1175	1.047
$h = 1/16$	2.972E-2	1.027	2.911E-2	1.040	2.902E-2	1.041
$h = 1/32$	7.197E-3	1.017	7.041E-3	1.028	7.013E-3	1.029
$h = 1/64$	1.773E-3	1.017	1.731E-3	1.029	1.722E-3	1.030

TABLE 23
FMG(6W(1,0))G_2 *functional norm errors and their ratios with corresponding discretization errors for the pure displacement problem.*

	$\lambda = 10$		$\lambda = 100$		$\lambda = 1000$	
	$G_2^{1/2}$	ratio	$G_2^{1/2}$	ratio	$G_2^{1/2}$	ratio
$h = 1/4$	0.2066	1.007	0.2104	1.007	0.2108	1.007
$h = 1/8$	5.161E-2	1.007	5.301E-2	1.006	5.318E-2	1.006
$h = 1/16$	1.288E-2	1.005	1.329E-2	1.005	1.335E-2	1.005
$h = 1/32$	3.245E-3	1.012	3.362E-3	1.014	3.378E-3	1.014
$h = 1/64$	8.495E-4	1.059	8.881E-4	1.071	8.933E-4	1.072

We again focus on MG based on G_2. The Stokes minimization problem is given by

$$\mathbf{V} = \operatorname{argmin}\{G_2(\mathbf{W};\mathbf{f}) : \mathbf{W} \in [H^1(\Omega)]^4, \mathbf{n}\cdot B\mathbf{W} = \mathbf{0} \text{ on } \Gamma_T, \quad \boldsymbol{\tau}\cdot QD\mathbf{W} = 0 \text{ on } \Gamma_D\}\,. \tag{15}$$

For the unit square, the boundary conditions in (15) are

$$\begin{aligned} &\left(1+\frac{1}{\lambda}\right)V_1 + V_4 = 0, \quad V_2 + V_3 = 0 \quad \text{on} \quad \Gamma_E\,,\\ &\frac{1}{\lambda}V_1 - V_4 = 0, \qquad V_2 = 0 \quad \text{on} \quad \Gamma_W\,,\\ &\frac{1}{\lambda}V_1 + V_4 = 0, \qquad V_3 = 0 \quad \text{on} \quad \Gamma_S\,,\\ &\left(1+\frac{1}{\lambda}\right)V_1 - V_4 = 0, \quad V_2 + V_3 = 0 \quad \text{on} \quad \Gamma_N\,. \end{aligned} \tag{16}$$

The numerical results given in Tables 24 through 27 show that the MG convergence factors are independent of λ. Again, the V cycle factors do not settle down as h is decreased as well as they did for pure traction, but they do a little better than that for pure displacement. Similarly, more relaxation and more coarse grid work appears to be worthwhile. Finally, Figure 5 represents the errors after 20 V(1,0) cycles for $h = \frac{1}{32}$ and $\lambda = 1000$. Similar to the pure displacement problem, MG for FOSLS based on G_2 produces errors that have predominantly smooth components, except near the boundaries. Again, our attempts to improve V cycle performance could not compete with the simpler W(1,0) cycle results, which appear to be independent of h.

5.7. Mixed boundary conditions: Discretization errors and FMG performance. To measure the discretization error, we take the same (smooth) functions $\mathbf{u}$, $\mathbf{V}$, and $\mathbf{f}$ as in section 5.5, noting that $\mathbf{V}$ satisfies the mixed boundary condition in

TABLE 24
Convergence factors for $V(1,0)$ based on G_2 for the mixed boundary value problem.

	$h=\frac{1}{4}$	$h=\frac{1}{8}$	$h=\frac{1}{16}$	$h=\frac{1}{32}$
$\lambda=10$	0.5609	0.6589	0.8086	0.8203
$\lambda=100$	0.5622	0.6369	0.8338	0.8293
$\lambda=1000$	0.5620	0.6470	0.8363	0.8289

TABLE 25
Convergence factors for $V(1,1)$ based on G_2 for the mixed boundary value problem.

	$h=\frac{1}{4}$	$h=\frac{1}{8}$	$h=\frac{1}{16}$	$h=\frac{1}{32}$
$\lambda=10$	0.3943	0.6167	0.7119	0.7604
$\lambda=100$	0.4040	0.6503	0.7509	0.8002
$\lambda=1000$	0.4049	0.6538	0.7550	0.8042

TABLE 26
Convergence factors for $V(2,1)$ based on G_2 for the mixed boundary value problem.

	$h=\frac{1}{4}$	$h=\frac{1}{8}$	$h=\frac{1}{16}$	$h=\frac{1}{32}$
$\lambda=10$	0.2939	0.5376	0.6482	0.6742
$\lambda=100$	0.3101	0.5742	0.6940	0.7103
$\lambda=1000$	0.3115	0.5781	0.6990	0.7062

TABLE 27
Convergence factors for $W(1,0)$ based on G_2 for the mixed boundary value problem.

	$h=\frac{1}{4}$	$h=\frac{1}{8}$	$h=\frac{1}{16}$	$h=\frac{1}{32}$
$\lambda=10$	0.5609	0.5925	0.6258	0.6080
$\lambda=100$	0.5622	0.6318	0.6434	0.6359
$\lambda=1000$	0.5620	0.6362	0.6452	0.6393

(1). With this $\mathbf{f}$, we found the approximate solution of (15) using 40 W(1,0) cycles on various levels of discretization. Tables 28 and 29 show that the relative discretization errors are also $O(h^2)$ with respect to both the L^2 and the G_2 functional norms ($G_2^{1/2}$).

To test overall accuracy for full multigrid, we studied FMG based on 6 V(1,0) cycles. Again, Tables 30 and 31 show that FMG(6V(1,0)) produces a total error comparing favorably to the discretization errors estimated in Tables 20 and 21. This implies that the problem on level h can be solved to within the level of discretization error at a cost of about $4/3 \cdot 6V(1,0) = 8$ V(1,0) cycles on level k, regardless of the size of λ.

6. Conclusion and remarks. Our numerical study confirms the theory in [6, 7, 8] by showing that both FOSLS approaches to planar linear elasticity achieve optimal finite element and multigrid performance even near the incompressible limit. Both approaches yield essentially the same λ-uniform optimal discretization accuracy, but the Stokes approach enables somewhat faster multigrid convergence. The results for pure traction with simple V cycles are not far from what is observed for multigrid

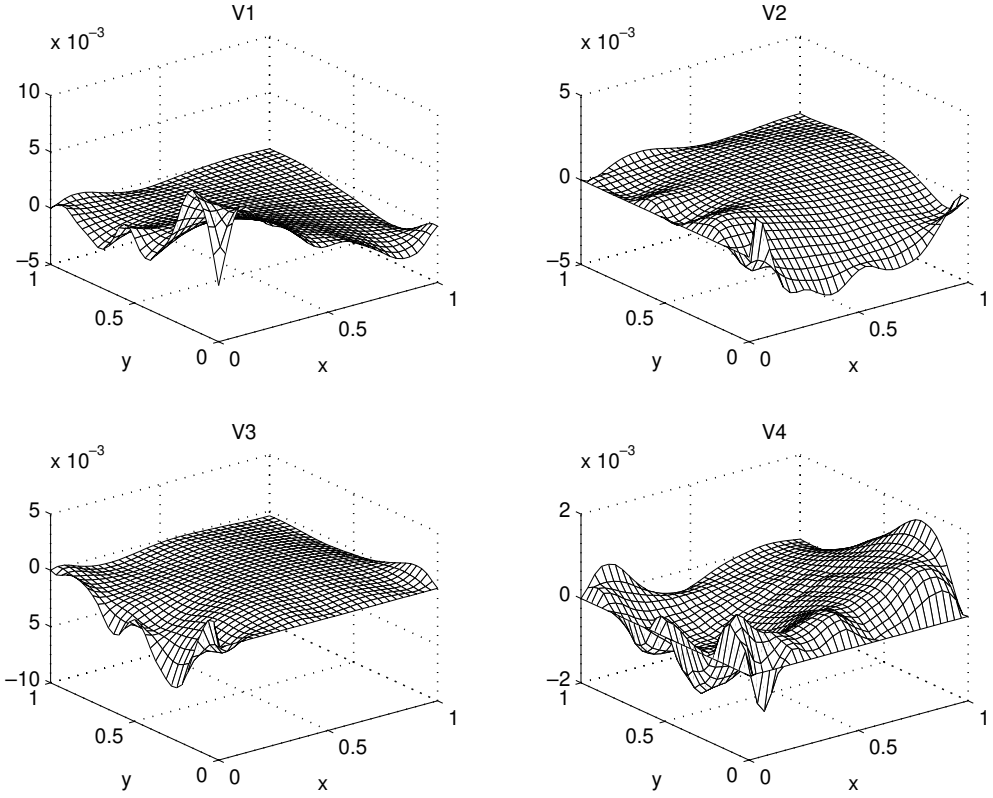

FIG. 5. *Errors after* 20 $V(1,0)$ *cycles based on* G_2 *for the mixed boundary value problem.*

TABLE 28

Discretization errors in the L^2 *norm and their convergence factors for the mixed boundary value problem.*

	$\lambda = 10$		$\lambda = 100$		$\lambda = 1000$	
	L^2 norm	factor	L^2 norm	factor	L^2 norm	factor
$h = 1/4$	0.7791		0.6854		0.6754	
$h = 1/8$	0.1656	0.2126	0.1490	0.2173	0.1474	0.2185
$h = 1/16$	3.514E-2	0.2122	3.318E-2	0.2227	3.305E-2	0.2242
$h = 1/32$	7.861E-3	0.2237	7.736E-3	0.2332	7.746E-3	0.2344
$h = 1/64$	1.846E-3	0.2348	1.857E-3	0.2400	1.865E-3	0.2408

TABLE 29

Discretization errors in the G_2 *functional norm and their convergence factors for the mixed boundary value problem.*

	$\lambda = 10$		$\lambda = 100$		$\lambda = 1000$	
	$G_2^{1/2}$	factor	$G_2^{1/2}$	factor	$G_2^{1/2}$	factor
$h = 1/4$	0.2075		0.2092		0.2094	
$h = 1/8$	5.118E-2	0.2467	5.180E-2	0.2476	5.190E-2	0.2479
$h = 1/16$	1.263E-2	0.2468	1.284E-2	0.2479	1.288E-2	0.2482
$h = 1/32$	3.125E-3	0.2474	3.188E-3	0.2483	3.200E-3	0.2484
$h = 1/64$	7.762E-4	0.2484	7.934E-4	0.2489	7.966E-3	0.2489

TABLE 30

FMG($6\mathsf{W}(1,0)$)L^2 *norm errors and their ratios with corresponding discretization errors for the mixed boundary value problem.*

	$\lambda = 10$		$\lambda = 100$		$\lambda = 1000$	
	L^2 norm	ratio	L^2 norm	ratio	L^2 norm	ratio
$h = 1/4$	0.7865	1.009	0.6928	1.011	0.6829	1.011
$h = 1/8$	0.1707	1.031	0.1541	1.034	0.1525	1.035
$h = 1/16$	3.604E-2	1.026	3.462E-2	1.043	3.455E-2	1.045
$h = 1/32$	7.971E-3	1.014	7.966E-3	1.030	7.993E-3	1.032
$h = 1/64$	1.868E-3	1.012	1.899E-3	1.023	1.908E-3	1.023

TABLE 31

FMG($6\mathsf{W}(1,0)$)G_2 *functional norm errors and their ratios with corresponding discretization errors for the mixed boundary value problem.*

	$\lambda = 10$		$\lambda = 100$		$\lambda = 1000$	
	$G_2^{1/2}$	ratio	$G_2^{1/2}$	ratio	$G_2^{1/2}$	ratio
$h = 1/4$	0.2083	1.004	0.2101	1.004	0.2104	1.005
$h = 1/8$	5.151E-2	1.006	5.217E-2	1.007	5.227E-2	1.007
$h = 1/16$	1.271E-2	1.006	1.296E-2	1.009	1.300E-2	1.009
$h = 1/32$	3.162E-3	1.012	3.240E-3	1.016	3.254E-3	1.017
$h = 1/64$	8.221E-4	1.059	8.508E-4	1.072	8.556E-4	1.074

methods applied to typical Poisson problems. The results for V cycle schemes for pure displacement and mixed boundary conditions are less remarkable, but W cycles are able to restore Poisson-like factors. In any case, the overall performance of the FOSLS methods studied here appears to be optimal uniformly in the Lamé constants, and it represents significant improvement over conventional methods (compared to the results in [2], for example).

REFERENCES

[1] I. BABUŠKA AND B. SZABO, *On the rates of convergence of the finite element method*, Internat. J. Numer. Methods Engrg., 18 (1982), pp. 323–341.

[2] S. C. BRENNER, *A nonconforming mixed multigrid method for the pure traction problem in planar linear elasticity*, Math. Comp., 63 (1994), pp. 435–460, S1–S5.

[3] S. C. BRENNER, *Multigrid methods for parameter dependent problems*, RAIRO Modél. Math. Anal. Numér, 54 (1996), pp. 265–297.

[4] S. C. BRENNER AND L. Y. SUNG, *Linear finite element methods for planar linear elasticity*, Math. Comp, 59 (1992), pp. 321–338.

[5] W. L. BRIGGS, V. E. HENSON, AND S. F. MCCORMICK, *A Multigrid Tutorial*, 2nd ed., SIAM, Philadelphia, 2000, to appear.

[6] Z. CAI, C.-O. LEE, T. A. MANTEUFFEL, AND S. F. MCCORMICK, *First-order system least squares for the Stokes and linear elasticity equations: Further results*, SIAM J. Sci. Comput., 21 (2000), pp. 1728–1739.

[7] Z. CAI, T. A. MANTEUFFEL, AND S. F. MCCORMICK, *First-order system least squares for the Stokes equations, with application to linear elasticity*, SIAM J. Numer. Anal., 34 (1997), pp. 1727–1741.

[8] Z. CAI, T. A. MANTEUFFEL, S. F. MCCORMICK, AND S. PARTER, *First-order system least squares (FOSLS) for planar linear elasticity: pure traction problem*, SIAM J. Numer. Anal., 35 (1998), pp. 320–335.

[9] C. L. CHANG, *A least-squares finite element method for the Helmholtz equation*, Comput. Methods Appl. Mech. Engrg., 83 (1990), pp. 1–7.

[10] P. CIARLET, *The Finite Element Method for Elliptic Problems*, North-Holland, Amsterdam, 1978.

[11] J. DOUGLAS AND J. WANG, *An absolutely stabilized finite element method for the Stokes problem*, Math. Comp., 52 (1989), pp. 495–508.

[12] C.-O. Lee, *A conforming mixed finite element method for the pure traction problem of linear elasticity*, Appl. Math. Comp., 93 (1998), pp. 11–29.

[13] P. Podio-Guidugli and G. Vergara-Caffarelli, *On a class of live traction problems in elasticity*, in Trends and Applications of Pure Mathematics to Mechanics, P. Ciarlet and M. Roseau, eds., Lecture Notes in Phys., Springer, Berlin, New York, 1995, pp. 291–304.

[14] R. Stenberg, *A family of mixed finite elements for the elasticity problem*, Numer. Math., 53 (1988), pp. 513–538.

[15] M. Vogelius, *An analysis of the p-version of the finite element method for nearly incompressible materials: uniformly valid, optimal error estimates*, Numer. Math., 41 (1983), pp. 39–53.